$\overline{\text{P}}$anda-MVD - note 001

# Parameterization of Energy Loss Distribution of Fast Charged Particles

Oscar Reinecke
René Jäkel

1/9/2008

**Abstract**

As particles go through matter they are decelerated by the quasi-free electrons therein. The measurement of this energy loss can be used to contribute to the global particle identification (PID) procedure especially in the low momentum region where the Bethe-Bloch is sufficiently mass-dependent. It is because of the statistic nature of the electron recoil that the energy loss is rather a stochastic quantity than a precisely defined value and it complies with the Landau probability distribution function (p.d.f.). Furthermore, the form of the p.d.f is changing with momentum and altered by measurement uncertainties.

For the calculation of consistent PID likelihoods, knowlege and numerically cost-effective reproduction of this p.d.f. is essential. A crafty method that fulfills these demands is introduced in this paper.

# 1 Simulation of the expected energy loss information

Interaction of various particle types with the PANDA-MVD has been simulated using the GEANT4 transport code as part of the PANDA simulation framework[1] and Kalman track refitting. Simulated data includes energy loss $S$, momentum $p$ and Monte Carlo particle ID of every track, generated by 50k single particles of 0.05 up to 1.2 GeV/$c$ momentum with isotropic angular distribution. The deposited energy $\mathrm{d}E_i$, the path-length $\mathrm{d}x_i$ (both within the traversed detector layer $i$), as well as the particle momentum have been calculated using the reconstructed track instead of the Monte Carlo track information. This allows to include the momentum uncertainty from the full track fit in the analysis.

Contrary to the usual method of summing the individual hit measurements $\mathrm{d}E_i/\mathrm{d}x_i$ to an energy loss information $\mathrm{d}E/\mathrm{d}x = \sum_i^n \mathrm{d}E_i/\mathrm{d}x_i$ all hit measurements can be combined to a total quantity

$$S = \frac{\sum \mathrm{d}E_i}{\sum \mathrm{d}x_i} \cdot n_\mathrm{e}^{-1} \tag{1}$$

In formula 1 the total energy loss per path length of the particle through the sensor material is divided by the electron density $n_\mathrm{e}$ of the detector material in order to be consistent with equation 2. Since the number of contributing hit points per track is small, usually not more than four hits in the barrel and up to six hits in the disc section contribute to the MVD PID information. This corresponds to only a few hundreds $\mu$m of silicon in total not sufficient to suppress the Landau tail of the energy loss distribution by a truncated mean method, for which the largest contributions to the total signal are neglected. Figure 1 shows the distribution for various charged particles.

[1] using the Babar like framework for data collection and root as analysis tool; code already accessible in the PandaRoot framework.

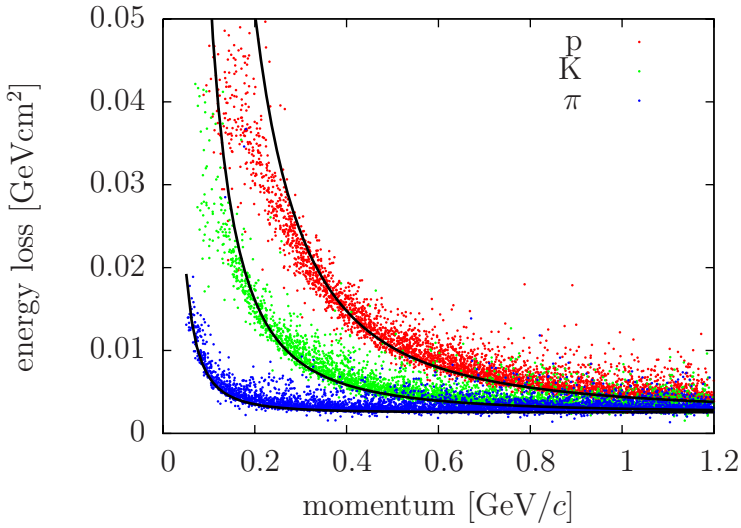


**Figure 1:** Distribution of energy losses for various particles after track reconstruction. At low momenta the mean value diverges from the Bethe-Bloch formula expectation (black lines) as given by eq. 2.

## 2 Parameterization of the energy loss distribution

The average energy loss obeys the well known Bethe-Bloch formula

$$\bar{S}(p) = (\alpha\hbar c)^2 \frac{4\pi}{m_e c^2} \cdot \beta^{-2} \left( \ln \left[ \frac{2 m_e c^2 \cdot \beta^2}{I(1-\beta^2)} \right] - \beta^2 \right) \tag{2}$$

without corrections for momenta below a few MeV/c. Those particles would get stopped within the MVD and would not leave a track in the detector. The velocity of the particle is defined as $\beta(p,m) = p/E$. The excitation potential for silicon is $I = 140$ eV. Due to the pion hypothesis used in the track reconstruction, the energy loss at low momenta differs from the theoretical prediction for other particle species. However, the shift of the distribution along a small interval can be corrected when fits are applied to a Bethe-Bloch-related energy loss $s = S - \bar{S}$ instead of the energy loss $S$ itself.

To reproduce the distribution, in the fit all measurement uncertainties are merged into a single Gaussian error that is added to the already Landau-distributed energy loss. The emerging distribution has to be calculated using numerical integration and is visualized in Figure 2. Its parameters are $\sigma$ (Gauss width), $\tau$ (Landau width), $\hat{s}$ (most probable value of the Landau p.d.f.). For completeness the convolution integral is defined as follows:

$$w_{\hat{s},\tau,\sigma}(s) = \int L_\tau(x - \hat{s}) \cdot G_\sigma(s - x) \mathrm{d}x \tag{3}$$

using

$$G_\sigma(x) = \frac{1}{\sqrt{2\pi}\sigma} \cdot e^{-x^2/\sigma^2}$$

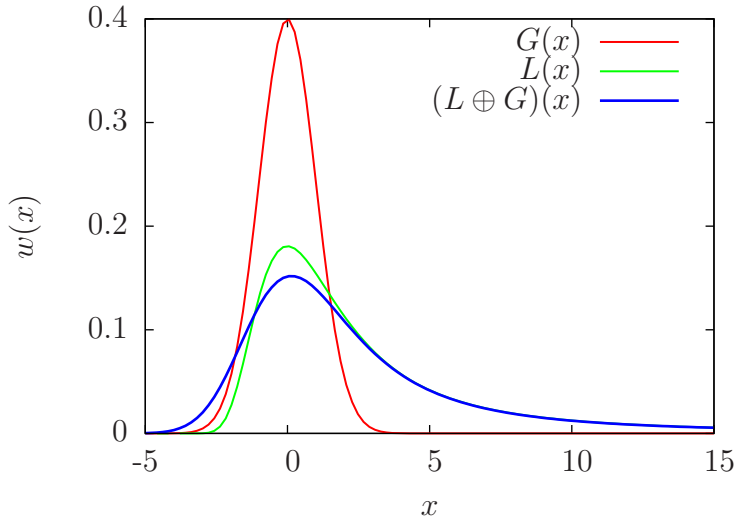


**Figure 2:** Convolution of a LANDAU- with a GAUSS distribution (blue line) i.e. the integral expression $w(s) = \int L(x) \cdot G(s-x)\mathrm{d}x$, both $L$ and $G$ have standard widths. The LANDAU distribution has its most probable value at $x = 0$.

as the GAUSSian distribution and

$$L_\tau(x) = \frac{1}{\pi\tau} \cdot \int_0^\infty e^{-t\ln t - t\cdot x/\tau} \sin(\pi t)\mathrm{d}t$$

for the scaled LANDAU distribution.

As an example, the signal model $w_{\hat{s},\tau,\sigma}(s)$ is applied to a sample of 800 MeV/c protons and the fit result is shown in Figure 3. Table 1 gives a comparison of the fit model to the energy loss distribution for two different momentum bins of width of 25 MeV/c, 400 MeV/c and 800 MeV/c, respectively. The third column represents

| momentum | parameter | $(\mathrm{d}E/\mathrm{d}x)_{\mathrm{total}}$ [MeVcm$^2$] | truncated $\mathrm{d}E/\mathrm{d}x$ |
|---|---|---|---|
| 400 MeV/c | $\tau$ | $0.149 \pm 0.018$ | $0.213 \pm 0.0184$ |
| | $\sigma$ | $1.052 \pm 0.031$ | $1.027 \pm 0.035$ |
| | $S$ | $12.37 \pm 0.040$ | $12.06 \pm 0.040$ |
| 800 MeV/c | $\tau$ | $0.238 \pm 0.011$ | $0.219 \pm 0.010$ |
| | $\sigma$ | $0.364 \pm 0.024$ | $0.354 \pm 0.021$ |
| | $S$ | $5.77 \pm 0.016$ | $5.65 \pm 0.015$ |

**Table 1:** Comparison of the fitting parameter for the $\mathrm{d}E/\mathrm{d}x$ signal for two different momentum bins.

the fit results for the total energy signal $(\mathrm{d}E/\mathrm{d}x)_{\mathrm{total}}$ compared to a truncated mean method, where the largest contribution of a hit was omitted. The latter method requires at least two hits in the MVD within the track fit. It has therefore a smaller efficiency. For the lower momentum the truncated mean method shows a larger

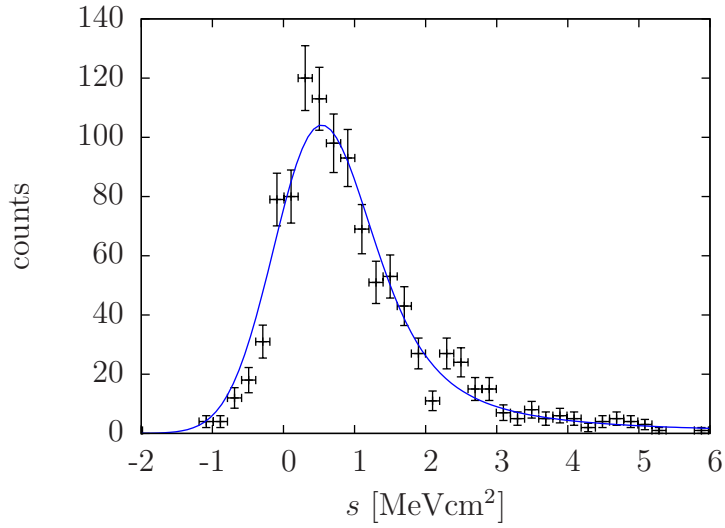


**Figure 3:** Proton energy loss distribution at $p = 0.8$ GeV/$c$ and its reproduced signal (blue line)

Landau width $\tau$, whereas the Gauss width $\sigma$ and the mean are comparable within the errors. Note that the most probable value $S$ for the distribution is given instead of the fit parameter $\hat{s}$ given in equation 3. Since the merged method to form the total quantity $(\mathrm{d}E/\mathrm{d}x)_{\mathrm{total}}$ in the relevant region of low momenta shows a narrow Landau width, this method has been used to calculate the probabilities for the various particle species.

# 3 Fitting and interpolation of the model parameters

The progression of the model parameters defined by equation 3 with momentum $p$ is determined by generating histograms of the Bethe-Bloch-related energy loss $s$ of all tracks whose momenta are within a $\Delta p = 25$ GeV/$c$ wide momentum bin over the full momentum range $p = 0.05 \ldots 2.0$ GeV/$c$. Afterwards, the parameters are most-likelihood fitted for each momentum bin. This gives the fitted parameters $\hat{s}_i$, $\sigma_i$, $\tau_i$ corresponding to $p_i$, and their covariances $\Delta\tau_i^2$, $\mathrm{Cov}(\sigma_i, \tau_i)$ etc. The parameters are shown in figure 4 in the relevant momentum range up to $p = 1.2$ GeV/$c$ for which the separation of various particle types is possible.

The fitted parameters are then interpolated with polynomials $\hat{s}(p)$, $\tau(p)$, $\sigma(p)$ that are defined as follows:

$$\hat{s}(p) = \begin{cases} c_0 + c_1 \cdot (p - p')[\mathrm{GeV}/c] & : p \geq p' \\ c_0 + c_1 \cdot (p - p')[\mathrm{GeV}/c] + \sum_{l \geq 3} c_l \cdot \{(p' - p)[\mathrm{GeV}/c]\}^l & : p < p' \end{cases} \tag{4}$$

The choice of $s(p)$ is derived more or less straight-forward from the appearance of the data points; there seems to be at most a linear dependance for $p \geq p'$ with suitably chosen $p'$ and the divergence at $p < p'$ is taken care of by a fifth order polynomial. The momentum is divided by 1 GeV/$c$ to avoid coefficients $c_l$ having

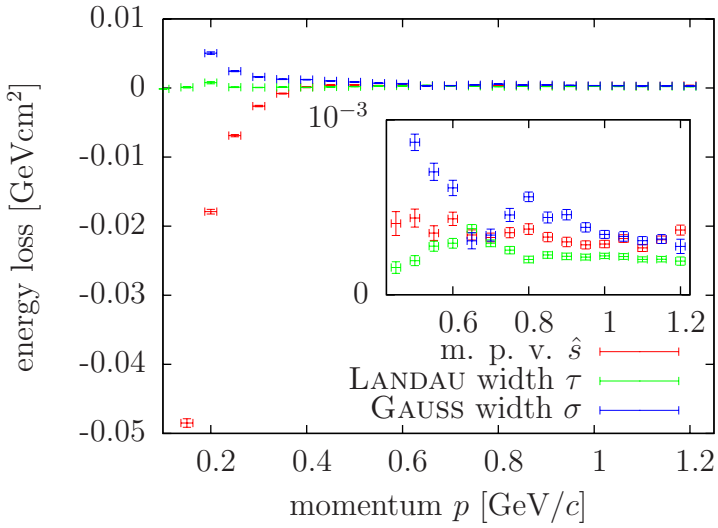


**Figure 4:** Progression of the distribution parameters for protons; The histograms used to fit the parameters are averaged over the depicted momentum errors. At $p \geq 0{,}6$ GeV/$c$ the statistical fluctuations between $\sigma$ and $\tau$ become aligned.

different units. Due to the low correlation between $\hat{s}_i$ and the remaining parameters, the coefficients are obtained from an ordinary least square fit.

Furthermore, the individual widths are parameterized with

$$\tau(p) = b_0 + b_1 \cdot p[\mathrm{GeV}/c] + b_2 \cdot \{p[\mathrm{GeV}/c]\}^2 \tag{5}$$

$$\sigma(p) = a_0 + a_1 \cdot p[\mathrm{GeV}/c] + a_n \cdot \{p[\mathrm{GeV}/c]\}^n \tag{6}$$

where $n$ is a negative integer used to handle the diverging GAUSSian uncertainty. Both widths are highly anti-correlated; for instance, a smaller GAUSS width is likely compensate for a higher LANDAU width. The correlation coefficients $\rho_i = \mathrm{Cov}(\tau_i,\sigma_i)/\Delta\tau_i\Delta\sigma_i$ are between -0.8 and -0.6. It is suggested that the quality of the interpolation improves when taking the correlation into account.

Fitting $\tau(p)$ and $\sigma(p)$ independently would yield to minimize

$$\chi^2_\tau = \frac{1}{2}\sum_i \left(\frac{\tau_i - \tau(p_i)}{\Delta\tau_i}\right)^2 \tag{7}$$

as well as

$$\chi^2_\sigma = \frac{1}{2}\sum_i \left(\frac{\sigma_i - \sigma(p_i)}{\Delta\sigma_i}\right)^2 \tag{8}$$

which would be the similiar to minimizing their sum

$$\chi'^2 = \chi^2_\tau + \chi^2_\sigma \tag{9}$$

with respect to $\sigma(p)$ and $\tau(p)$ at the same time. This is normally expressed as

$$\chi'^2 = \frac{1}{2}\sum_i \begin{pmatrix} \tau_i - \tau(p_i) \\ \sigma_i - \sigma(p_i) \end{pmatrix}^\dagger C_i'^{-1} \begin{pmatrix} \tau_i - \tau(p_i) \\ \sigma_i - \sigma(p_i) \end{pmatrix} \tag{10}$$

| | p | K | $\pi$ | $\mu$ | e |
|---|---|---|---|---|---|
| $p'$ [GeV/$c$] | 0.45 | 0.25 | 0.1 | 0.15 | 0 |
| $c_0$[MeVcm$^2$] | 0.383 | 0.326 | 0.275 | 0.249 | 2.9 |
| $c_1$[MeVcm$^2$] | -0.127 | -7.681 | 3.257 | 0.066 | 0.018 |
| $c_3$[GeVcm$^2$] | -3.058 | -19.662 | 0 | 4.332 | 0 |
| $c_4$[GeVcm$^2$] | 24.636 | 264.382 | 0 | -107.686 | 0 |
| $c_5$[GeVcm$^2$] | -68.632 | -1238.09 | -6624.05 | 699.522 | 0 |

**Table 2:** Coefficients for $\hat{s}(p)$ as in equation 4

where the introduced covariance matrix $C_i'$ of course has to be diagonal:

$$C_i' = \begin{pmatrix} \Delta\tau_i^2 & 0 \\ 0 & \Delta\sigma_i^2 \end{pmatrix} \tag{11}$$

Taking the correlation into account then means using the full covariance matrix

$$C_i = \begin{pmatrix} \Delta\tau_i^2 & \rho_i\Delta\tau_i\Delta\sigma_i \\ \rho_i\Delta\tau_i\Delta\sigma_i & \Delta\sigma_i^2 \end{pmatrix} \tag{12}$$

instead of $C_i'$, hence the quantity to be minimized is given by

$$\chi^2 = \frac{1}{2}\sum_i \begin{pmatrix} \tau_i - \tau(p_i) \\ \sigma_i - \sigma(p_i) \end{pmatrix}^\dagger \begin{pmatrix} \Delta\tau_i^2 & \rho_i\Delta\tau_i\Delta\sigma_i \\ \rho_i\Delta\tau_i\Delta\sigma_i & \Delta\sigma_i^2 \end{pmatrix}^{-1} \begin{pmatrix} \tau_i - \tau(p_i) \\ \sigma_i - \sigma(p_i) \end{pmatrix} \tag{13}$$

The inverse covariance matrix $C_i^{-1}$ can be written as

$$\begin{aligned} C_i^{-1} &= \left[\begin{pmatrix} \Delta\tau_i & 0 \\ 0 & \Delta\sigma_i \end{pmatrix}\begin{pmatrix} 1 & \rho_i \\ \rho_i & 1 \end{pmatrix}\begin{pmatrix} \Delta\tau_i & 0 \\ 0 & \Delta\sigma_i \end{pmatrix}\right]^{-1} \\ &= \begin{pmatrix} \Delta\tau_i^{-1} & 0 \\ 0 & \Delta\sigma_i^{-1} \end{pmatrix}\begin{pmatrix} 1 & -\rho_i \\ -\rho_i & 1 \end{pmatrix}\begin{pmatrix} \Delta\tau_i^{-1} & 0 \\ 0 & \Delta\sigma_i^{-1} \end{pmatrix}\frac{1}{1-\rho_i^2} \end{aligned} \tag{14}$$

and is therefore given analytically.

The minimization of equation 13 is done using `ROOT`[2]. All resulting coefficients are summarized in the tables 2 and 3. Figure 5 shows the momentum dependent width parameter $\sigma_i$ (full squares) and $\tau_i$ (open circles) and the interpolation curves for both parameters with respect to the particle momentum. The small inset in figure 5 shows the momentum bin marked by the black lines and the good agreement between the signal description using the interpolation functions for the model parameters (blue curve) and the data points (red curve). The same comparison is done in figure 3 for a higher momentum interval. The data are well described by using the interpolation curves for the model parameters.

The interpolation curves were than basis for the calculation of the likelihood for all particle hypotheses in the reconstruction process.

# 4 Separation ability of the MVD

To identify a particle the MVD might only contribute for low particle momenta, which can be seen e.g. in figure 1. At higher particle momenta, the MVD energy loss will be independent of the particle type and the individual bands start to overlap.

[2]and its minimization package `MINUIT`

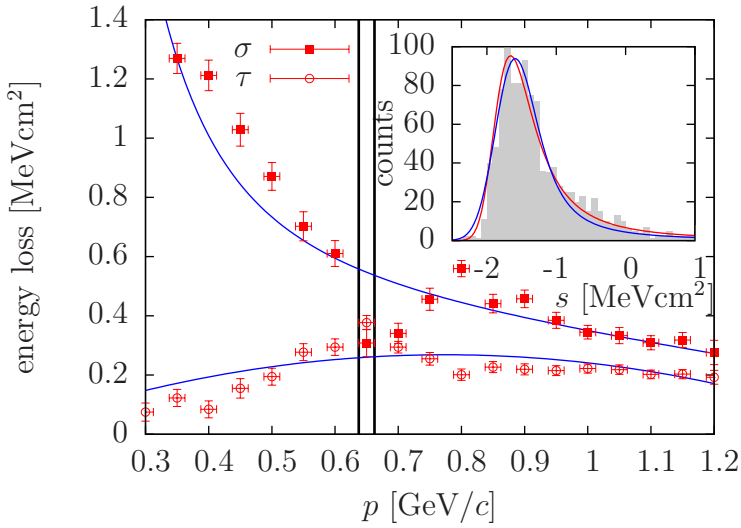


**Figure 5:** Proton parameter functions $\sigma(p)$, $\tau(p)$, distribution of the Bethe-Bloch-related energy loss $s = S - \bar{S}$ for the depicted interval; in the inset, the blue line shows the distribution generated by the interpolated parameters, whereas the red line corresponds to the fitted parameters.

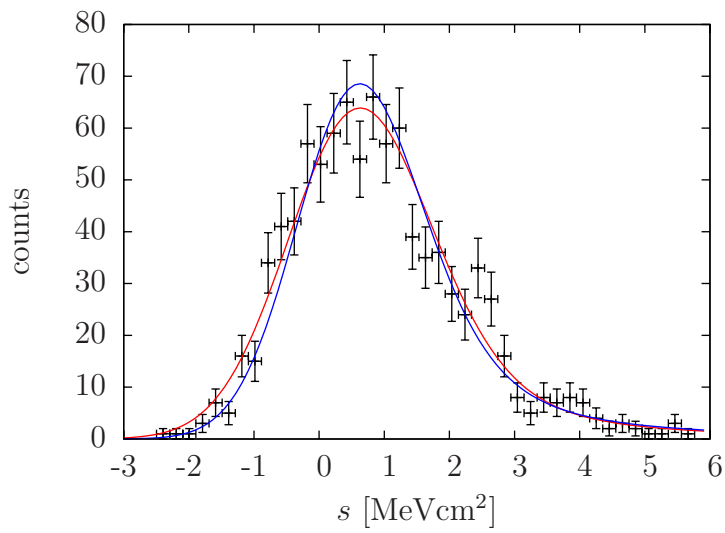


**Figure 6:** Proton energy loss distribution at $p = 0.45$ GeV/$c$

| | p | K | $\pi$ | $\mu$ | e |
|---|---|---|---|---|---|
| $b_0$[MeVcm$^2$] | -0.053 | 0.342 | 0.183 | 0.189 | 0.128 |
| $b_1$[MeVcm$^2$] | 0.830 | -0.321 | -0.128 | -0.146 | -3.157·10$^{-3}$ |
| $b_2$[MeVcm$^2$] | -0.536 | 0.137 | 0.080 | 0.091 | 9.647·10$^{-3}$ |

**Table 3:** Coefficients for $\tau(p)$ as in equation 5

| | p | K | $\pi$ | $\mu$ | e |
|---|---|---|---|---|---|
| $n$ | -3 | -3 | -2 | -2 | -3 |
| $a_0$ [MeVcm$^2$] | 0.640 | 0.387 | 0.223 | 0.167 | 0.409 |
| $a_1$ [MeVcm$^2$] | -0.322 | -0.162 | -3.214·10$^{-3}$ | 0.057 | -0.036 |
| $a_n$[keVcm$^2$] | 31.771 | 7.766 | 4.648 | 3.427 | 0.018 |

**Table 4:** Coefficients for $\sigma(p)$ as in equation 6

A usual way to compare the ability to separate individual distributions, e.g. the energy loss for different particle types in the same momentum bin, the calculation of the separation power gives a good approximation. The separation power $P$ is defined as follows:

$$P = \frac{s_1 - s_2}{\sigma_1/2 + \sigma_2/2}. \tag{15}$$

The $s_i$ are the fitted most probable values from the energy loss distributions and the $\sigma_i$ are the Gaussian widths for two different particle types. The separation power can be interpreted as the "number of Gaussian sigmas", which separate two Gaussian shaped distributions. As described in 2 the full energy loss signal from the MVD needs a Landau component to describe the data reasonable well. Figure 7 gives an overview of the magnitude of both width parameters with respect to the particle momentum.

At $p > 600$ MeV/c both widths become comparably large. To compensate the growing influence of the Landau contribution in the signal description the Gaussian width has been doubled and the separation power calculated. The result for all possible particle combinations for protons, kaons and pions is given in figure 8.

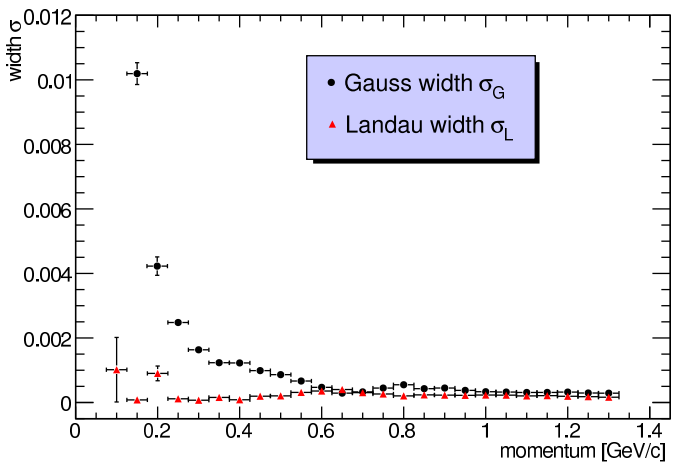


**Figure 7:** Momentum dependence of the Gaussian and Landau component of the energy loss distribution.

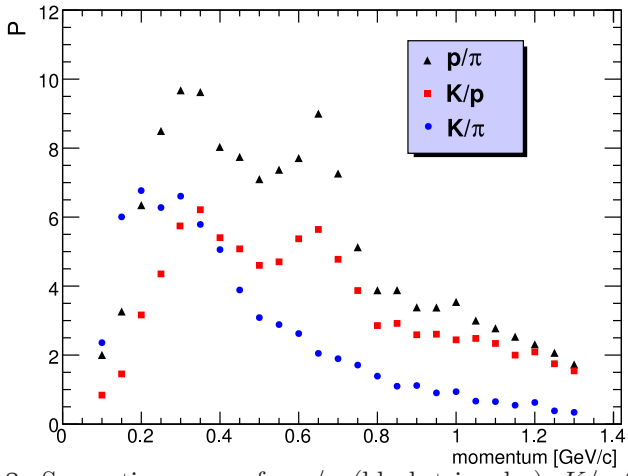


**Figure 8:** Separation power for $p/\pi$ (black triangles), $K/p$ (red squares) and $K/\pi$ (blue circles) separation and its evolution with momentum.

The separation of protons and pions is possible up to 1 GeV/c momentum with at least $3\sigma$ separation power. The same applies to kaon/proton separation up to 800 MeV/c as well as kaon/pion up to 400 MeV/c.

At larger momenta the LANDAU component in the description of the energy loss signal becomes large and the separation power is not sufficient to calculate the probability of identifying a particular particle type. Since the shape of the model parameter $\sigma$, $\tau$ and $s$ has been parameterized for each particle type, the probability for each type can be calculated for a given track and its associated MVD energy information. The strength of the energy loss distribution for all hypotheses is normalized and figure 9 shows the evolution of the normalized proton likelihood with momentum. The lower left figure shows the corresponding misidentification for a particle be recognized as kaon, or as pion, respectively in the lower right figure. The misidentification probabilities for muons and elecrons are the same as for pions.

Figure 10 show the same for kaon tracks. The corresponding misidentification probabilities for proton and pion hypothesis is shown in addition.

In general the MVD can contribute to the PID decision in the PANDA detector in the momentum range up to $\approx 0.6$ GeV/$c$ for kaons and up to $\approx 1$ GeV/$c$ for protons. The signals for electrons, pions and muons are too similar to contribute to the PID. Together with the outer tracking system, either STT or TPC, the combined PID information is complementary to the DIRC information starting at higher particle momenta and crucial for identifying low momentum particles.

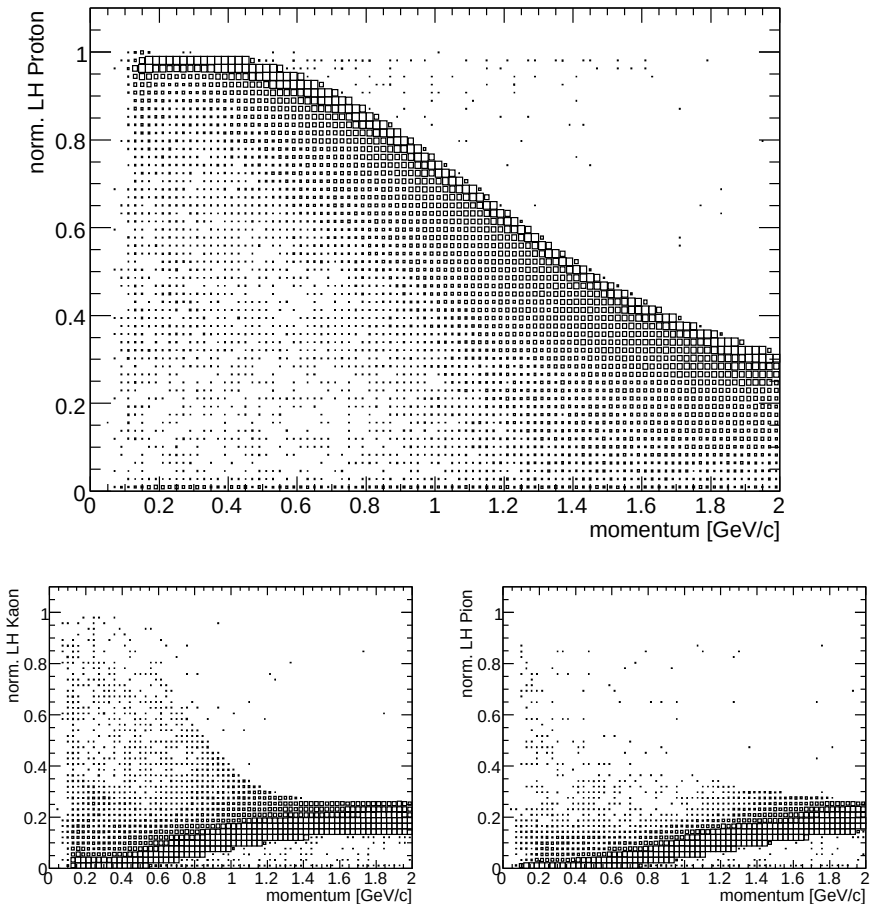


**Figure 9:** MVD probability scan over wide momentum range for proton tracks. The lower left picture shows the misidentification probability for assuming the particle to be a kaon (left) or pion (right).

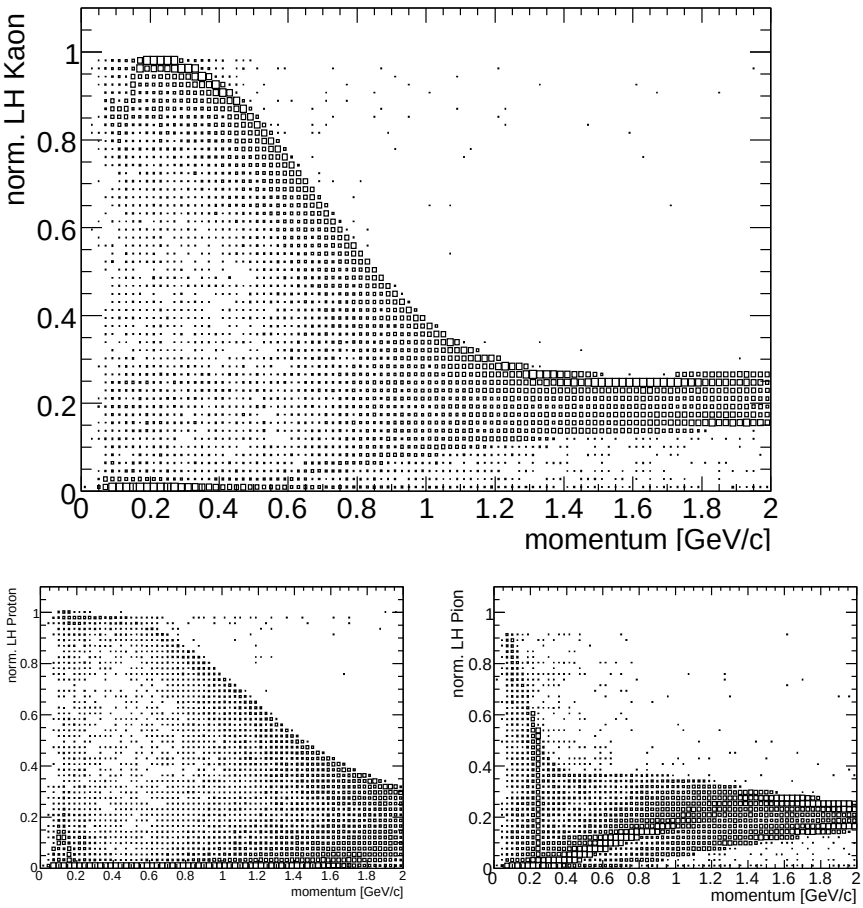


**Figure 10:** MVD probability scan over wide momentum range for kaon tracks. The lower left picture shows the misidentification probability for assuming the particle to be a proton (left) or pion (right).